Nonlinear δf particle simulations of collective excitations and energy-anisotropy instabilities in high-intensity bunched beams

Hong Qin, Ronald C. Davidson, and Edward A. Startsev
Plasma Physics Laboratory, Princeton University, Princeton, New Jersey 08543, USA
(Received 22 March 2007; published 6 June 2007)

Collective effects with strong coupling between the longitudinal and transverse dynamics are of fundamental importance for applications of high-intensity bunched beams. The self-consistent Vlasov-Maxwell equations are applied to high-intensity finite-length charge bunches, and a generalized δf particle simulation algorithm is developed for bunched beams with or without energy anisotropy. The nonlinear δf method exhibits minimal noise and accuracy problems in comparison with standard particle-in-cell simulations. Systematic studies are carried out under conditions corresponding to strong 3D nonlinear space-charge forces in the beam frame. For charge bunches with isotropic energy, finite bunch-length effects are clearly evident by the fact that the spectra for an infinitely long coasting beam and a nearly spherical charge bunch have strong similarities, whereas the spectra have distinctly different features when the bunch length is varied between these two limiting cases. For bunched beams with anisotropic energy, there exists no exact kinetic equilibrium because the particle dynamics do not conserve transverse energy and longitudinal energy separately. A reference state in approximate dynamic equilibrium has been constructed theoretically, and a quasi-steady state has been established in the simulations for the anisotropic case. Collective excitations relative to the reference state have been simulated using the generalized δf algorithm. In particular, the electrostatic Harris instability driven by strong energy anisotropy is investigated for a finite-length charge bunch. The observed growth rates are larger than those obtained for infinitely long coasting beams. However, the growth rate decreases for increasing bunch length to a value similar to the case of a long coasting beam. For long bunches, the instability is axially localized symmetrically relative to the beam center, and the characteristic wavelength in the longitudinal direction is comparable to the transverse dimension of the beam.

DOI: 10.1103/PhysRevSTAB.10.064201 PACS numbers: 29.27.Bd, 41.85.Ct, 41.85.Ew

I. INTRODUCTION

Collective effects in high-intensity charged particle beams are often manifest by collective excitations with certain dynamical properties such as instabilities and Landau damping [1–6]. In particular, collective effects with strong coupling between the longitudinal and transverse dynamics are of fundamental importance for the applications of high-intensity bunched beams [7,8]. One of the active research areas where it is necessary to systematically study this transverse and longitudinal coupling is the neutralized drift compression experiment (NDCX) [9]. The NDCX research program is focused on the capability of compressing heavy ion charge bunches both longitudinally and transversely [10–12] to reach the high intensity and short pulse length required for creating high energy density matter and heavy ion fusion conditions in the laboratory [13,14]. Obviously, transverse and longitudinal coupling constitutes an important aspect of the compression dynamics. The self-consistent theoretical framework for studying collective effects is provided by the nonlinear Vlasov-Maxwell equations [3,15,16]. A corresponding numerical method, the δf particle simulation method, has been developed [17] to solve the nonlinear Vlasov-Maxwell equations with significantly reduced noise. This theoretical and numerical framework has been successfully applied to study stable beam propagation [18], electron-ion two-stream (electron cloud) instabilities [19–29], and collective instabilities driven by large energy anisotropy [30–33]. However, previous studies were carried out primarily for long coasting beams with a strong nonlinear space-charge field in the transverse direction. In this paper, we report recent progress in developing a generalized nonlinear δf simulation method to study collective effects for finite-length charge bunches with nonlinear space-charge fields in both the longitudinal and transverse directions.

For high-intensity bunched beams, the equilibrium and collective excitation properties are qualitatively different from those for coasting beams. Here, the most interesting physics is the coupling between the transverse and longitudinal dynamics induced by the nonlinear space-charge forces in a finite-length charge bunch. One objective of this paper is to numerically analyze, by using the δf simulation method, the interplay between finite bunch length and the space-charge fields on the eigenmodes of collective excitations for bunched beams with isotropic energy. For simplicity of presentation, the present analysis is carried out in the beam frame. Another consequence of the coupling effect in a finite-length charge bunch is that the particle dynamics does not conserve transverse energy and longitudinal energy separately, and there exists no exact kinetic equilibrium $(\partial/\partial t = 0)$ which has anisotropic energy in

the transverse and longitudinal directions. On the other hand, for charged particle beams accelerated to high energy, energy anisotropy in the beam frame develops naturally as a result of phase space volume conservation [2]. Previous studies have shown that the nonintegrability induced by the coupling between the longitudinal and transverse dynamics is relatively weak, even for high-intensity beams [34–36]. Based on this fact, we have developed a reference state for beams with anisotropic energy, which is not an exact, but an approximate equilibrium solution of the Vlasov-Maxwell equations. The difference between the exact solution and the reference state is simulated by the generalized δf particle simulation algorithm described in this paper. As an important application of the generalized δf method, numerical simulations of the electrostatic Harris instability driven by large energy anisotropy are carried out. The effects of finite bunch length are investigated, and the results are compared with previous simulation results for infinitely long coasting beams.

The paper is organized as follows. After the development of the generalized δf particle simulation algorithm in Sec. II, collective excitations in bunched beams with isotropic energy are studied in Sec. III. Then, in Sec. IV, the reference state for bunched beams with temperature anisotropy is constructed, and properties of the anisotropy-driven instability are investigated.

II. THEORETICAL MODEL AND THE GENERALIZED δf SIMULATION METHOD

We consider a single-species, bunched beam confined in both the r and z directions by an external smooth-focusing force in the beam frame

$$\mathbf{F}_{\mathrm{foc}} = -m\omega_\perp^2 \mathbf{x}_\perp - m\omega_z^2 z \mathbf{e}_z. \tag{1}$$

Here, $\omega_\perp$ and ω_z are the constant transverse and longitudinal applied focusing frequencies in the smooth-focusing approximation. In the beam frame, the dynamics of the bunched beam is described by the nonlinear Vlasov-Maxwell equations [3]

$$\left\{\frac{\partial}{\partial t} + \mathbf{v}\cdot\frac{\partial}{\partial \mathbf{x}} - \left[m(\omega_\perp^2 \mathbf{x}_\perp + \omega_z^2 z\mathbf{e}_z) + e\left(\nabla\phi - \frac{v_z}{c}\nabla_\perp A_z\right)\right]\cdot\frac{\partial}{\partial \mathbf{p}}\right\} f(\mathbf{x},\mathbf{p},t) = 0, \tag{2}$$

$$\nabla^2\phi = -4\pi e\int d^3p\, f(\mathbf{x},\mathbf{p},t), \tag{3}$$

$$\nabla^2 A_z = -\frac{4\pi}{c}e\int d^3p\, v_z f(\mathbf{x},\mathbf{p},t), \tag{4}$$

where f is particle distribution function in phase space, and e and m are the particle charge and rest mass, respectively.

This set of equations is a simplified version of the nonlinear Vlasov-Maxwell equations in the general case [3,25]. For boundary conditions, a perfectly conducting cylindrical pipe is located at radius $r = r_w$, and periodic boundary conditions are adopted in the longitudinal direction. The simulation dimension in the longitudinal direction is between $z = -z_{\max}$ and $z = z_{\max}$. Since Eqs. (2)–(4) form a nonlinear integrodifferential system, analytical techniques for solving Eqs. (2)–(4) are limited. Systematic studies of the nonlinear dynamics determined by Eqs. (2)–(4) require an effective numerical tool. For this purpose, we use the low-noise nonlinear δf method [17,23,24]. The total distribution function is divided into two parts, $f = f_0 + \delta f$, where f_0 is a *known reference* distribution function, and the numerical simulation is carried out to determine the detailed nonlinear evolution of the perturbed distribution function δf. This is accomplished by advancing the weight function defined by $w \equiv \delta f/f$. The dynamical equation for w is given by

$$\frac{dw}{dt} = -(1-w)\frac{1}{f_0}\left[\left(\frac{df_0}{dt}\right)_\delta + \left(\frac{df_0}{dt}\right)_0\right], \tag{5}$$

where

$$\left(\frac{df_0}{dt}\right)_\delta = -e(\nabla\delta\phi - \frac{v_z}{c}\nabla_\perp\delta A_z)\cdot\frac{\partial f_0}{\partial \mathbf{p}}, \tag{6}$$

$$\left(\frac{df_0}{dt}\right)_0 = \left\{\frac{\partial}{\partial t} + \mathbf{v}\cdot\frac{\partial}{\partial \mathbf{x}} - \left[m(\omega_\beta^2\mathbf{x}_\perp + \omega_z^2 z\mathbf{e}_z) + e\left(\nabla\phi_0 - \frac{v_z}{c}\nabla_\perp A_{z0}\right)\right]\cdot\frac{\partial}{\partial \mathbf{p}}\right\} f_0. \tag{7}$$

Here, $\delta\phi \equiv \phi - \phi_0$ and $\delta A_z \equiv A_z - A_{z0}$. For the perturbed fields, Maxwell's equations are given by

$$\nabla^2\delta\phi = -4\pi e\int d^3p\, w f(\mathbf{x},\mathbf{p},t), \tag{8}$$

$$\nabla^2\delta A_z = -\frac{4\pi}{c}e\int d^3p\, v_z w f(\mathbf{x},\mathbf{p},t), \tag{9}$$

where the reference potentials (ϕ_0, A_{z0}) are chosen to satisfy

$$\nabla^2\phi_0 = -4\pi e\int d^3p\, f_0(\mathbf{x},\mathbf{p},t), \tag{10}$$

$$\nabla^2 A_{z0} = -\frac{4\pi}{c}e\int d^3p\, v_z f_0(\mathbf{x},\mathbf{p},t). \tag{11}$$

It is desirable to pick (ϕ_0, A_{z0}, f_0) as self-consistent solutions to the Vlasov-Maxwell equations (2)–(4), such that the $(df_0/dt)_0$ term in Eq. (5) vanishes. For most applications, (ϕ_0, A_{z0}, f_0) are chosen to correspond to an equilibrium solution with $\partial/\partial t = 0$, and the generalized δf particle simulation algorithm reduces to the standard nonlinear δf method [24]. For bunched beams, if the energy is isotropic in the beam frame, the reference state can be chosen to be an exact equilibrium solution. However, for bunched beams with energy anisotropy, exact

equilibrium solutions do not exist due to the lack of independent longitudinal and transverse invariants of the particle dynamics, and we can only choose a reference distribution f_0 that is close to a quasiequilibrium state. Furthermore, for a single-species beam, we neglect A_z in the beam frame because $|A_z| \ll |\phi|$.

The nonlinear particle simulations are carried out by iteratively advancing the particle motions and momenta, including the weights they carry according to Eq. (5), and updating the fields by solving the perturbed Maxwell's equations (8) and (9). Even though it is a perturbative approach, the δf method is *fully nonlinear* and simulates completely the original nonlinear Vlasov-Maxwell equations. Compared with conventional particle-in-cell simulations, the noise level in δf simulations is significantly reduced. The δf method reduces the noise level of the simulations because the statistical noise for the total distribution function in the conventional particle-in-cell (PIC) method is only associated with the perturbed distribution function in the δf method . If the same number of simulation particles is used in the two approaches, then the noise level in the δf method is reduced by a factor of $f/\delta f$ relative to the PIC method. To achieve the same accuracy for the perturbed fields, the number of simulation particles used in the δf method is reduced by a factor of $(f/\delta f)^2$ [17,23,24]. The δf method can also be used to study *linear* eigenmode and stability properties, provided the factor $(1 - w)$ in Eq. (5) is approximated by unity, and particle orbits are advanced by the unperturbed force only.

III. COLLECTIVE EXCITATIONS FOR BUNCHED BEAMS WITH ISOTROPIC ENERGY

Since the conventional concept of collective excitations or eigenmodes of charged particle beams refers to perturbations around a self-consistent equilibrium, the first step in the present study is to identify possible equilibrium solution (ϕ_0, f_0) with $\partial/\partial t = 0$ satisfying

$$\left\{\mathbf{v}\cdot\frac{\partial}{\partial\mathbf{x}} - [m(\omega_\perp^2\mathbf{x}_\perp + \omega_z^2 z\mathbf{e}_z) + e\nabla\phi_0]\cdot\frac{\partial}{\partial\mathbf{p}}\right\} f_0(\mathbf{x},\mathbf{p}) = 0,$$

$$\nabla^2\phi_0 = -4\pi e\int d^3p f_0(\mathbf{x},\mathbf{p}). \tag{12}$$

In this section, we choose f_0 to be a function of the energy invariant H according to

$$f_0 = f_0(H) = \frac{\hat{n}}{(2\pi mT)^{3/2}}\exp\left(\frac{-H}{T}\right), \tag{13}$$

$$H = \frac{\mathbf{p}^2}{2m} + e\phi_0 + \frac{1}{2}m(\omega_\perp^2 r^2 + \omega_z^2 z^2). \tag{14}$$

Here, $\hat{n}$ is the beam number density at $(r, z) = (0, 0)$. Equation (13) gives a constant isotropic temperature $T =$ const. Under this assumption, the equilibrium Poisson equation (12) becomes

$$\nabla^2\phi_0 = -4\pi e\hat{n}\exp\left[-\frac{m(\omega_\perp^2 r^2 + \omega_z^2 z^2)}{2T} - \frac{e\phi_0}{T}\right], \tag{15}$$

which is to be solved for ϕ_0 in a perfectly conducting cylindrical pipe with wall radius r_w. It can be shown [3] that the condition for the beam to be confined by the applied focusing field is

$$s_b \le 1 + \frac{\omega_z^2}{2\omega_\perp^2}. \tag{16}$$

Here, the dimensionless parameter $s_b \equiv 4\pi\hat{n}e^2/2m\omega_\perp^2$ measures the relative strength of the space-charge force compared with the applied transverse focusing force. Even though the kinetic equilibrium is taken to be the well-known thermal equilibrium distribution in Eq. (13), the dynamics of a single particle on constant-energy surfaces is nonintegrable due to the coupling between the transverse and longitudinal dynamics induced by the 3D nonlinear space-charge force [35]. The coupling is a function of the space-charge strength and the bunch length. When the space-charge intensity is reduced to zero, or the bunch length is increased to infinity, the transverse and longitudinal space-charge forces decouple and the particle dynamics is integrable [36]. Detailed studies of the chaotic

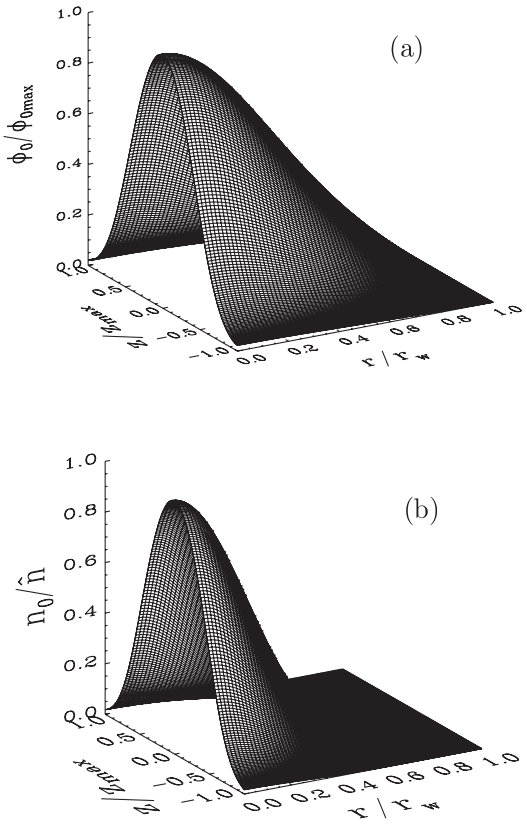

FIG. 1. Numerically solved equilibrium potential ϕ_0 and density n_0 profile as functions of (r, z) for a charge bunch with $s_b = 0.27$, $\omega_z/\omega_\perp = 0.074$, and $T_\perp/T_z = 1$. The aspect ratio of the charge bunch is $z_b/r_b = 10$.

behavior of the particle orbits can be found in Refs. [34–36].

The Poisson equation (15) can be readily solved numerically. Since the source term on the right-hand side of Eq. (15) depends on the potential nonlinearly, an iterative method is needed. Illustrated in Fig. 1 are the numerically solved equilibrium potential ϕ_0 and density profile n_0 as functions of (r, z) for a bunched beam with $s_b = 0.27$, $\omega_z/\omega_\perp = 0.074$, and $T_\perp/T_z = 1$. The aspect ratio of the charge bunch is $z_b/r_b = 10$, and $r_b/r_w = 0.35$. Here, the effective bunch size in the transverse direction (r_b) and that in the longitudinal direction (z_b) are defined by

$$r_b^2 = \frac{\int_0^{r_w} drr^3 n(r,0)}{\int_0^{r_w} drrn(r,0)}, \tag{17}$$

$$z_b^2 = \frac{\int_0^{\infty} dzz^2 n(0,z)}{\int_0^{\infty} dzn(0,z)}. \tag{18}$$

Next, we numerically study finite bunch-length effects on the linear eigenmodes of collective excitations for different space-charge intensities. In the simulations, an initial perturbation with an arbitrary dependence on r and z coordinates is introduced at $t = 0$. The system is evolved

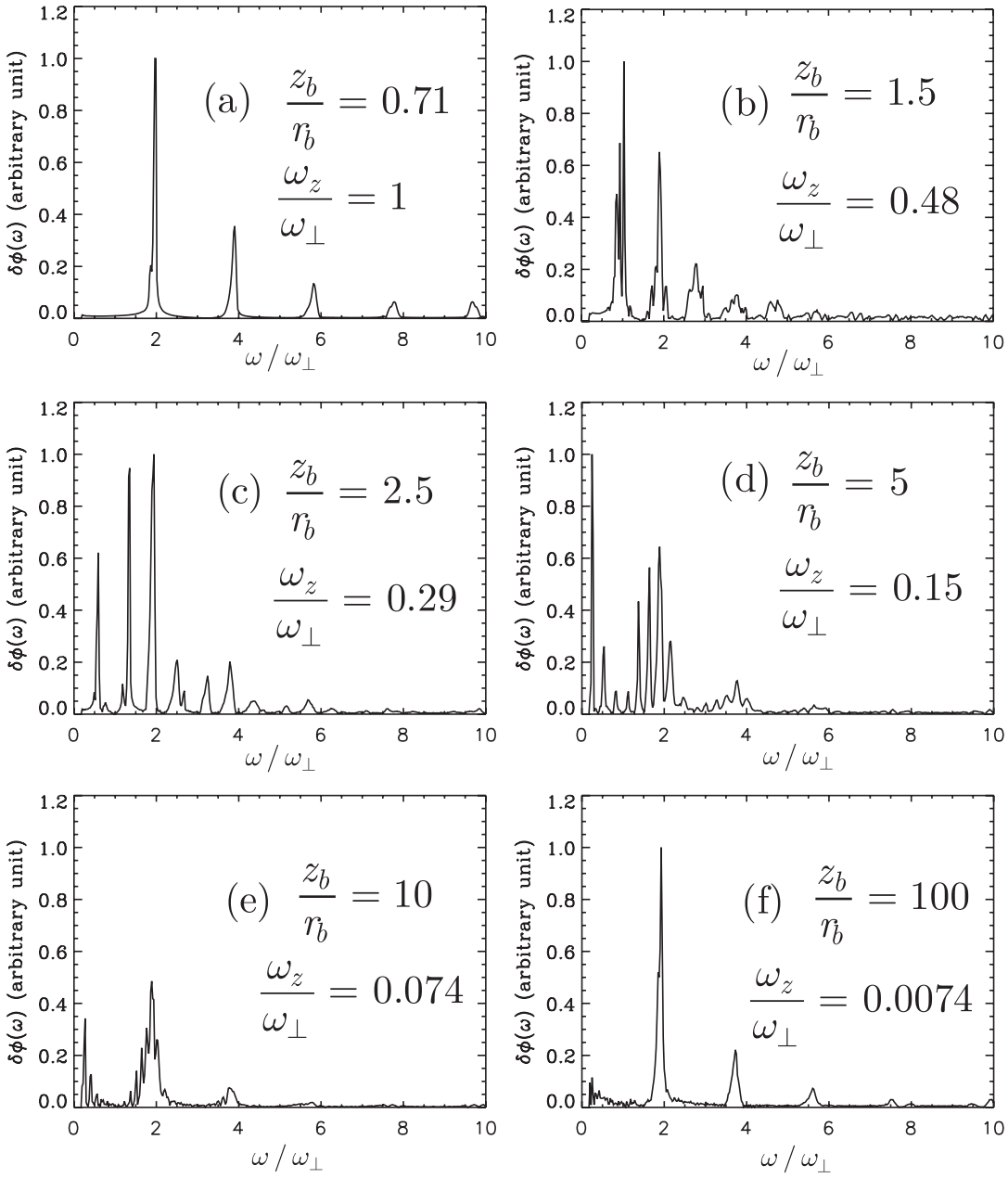

FIG. 2. Spectra of axisymmetric linear eigenmodes for bunched beams with normalized space-charge intensity $s_b = 0.27$ and different bunch aspect ratios $z_b/r_b = 0.71$, 1.5, 2.5, 5, 10, and 100. The values of r_b/r_w are kept at $r_b/r_w = 0.35$ for all cases.

using the linear δf algorithm described in Sec. II. For the results presented in this section, the simulations are carried out from $t = 0$ to $t = 250/\omega_\perp$. The simulations were performed on the IBM SP3 computer at the National Energy Research Scientific Computing Center with 128 processors, 10×10^6 particles, and 8×10^{10} particle $\times$ steps. Shown in Fig. 2 are the Fast-Fourier-Transformation spectra of the axisymmetric ($\partial/\partial\theta = 0$) linear eigenmodes obtained from the simulations for bunched beams with normalized space-charge intensity $s_b = 0.27$, but for different bunch aspect ratios, $z_b/r_b =$ 0.8, 1.5, 2.5, 5, 10, and 100. Figure 2(a) is the case where $\omega_\perp = \omega_z$, corresponding to a nearly spherical charge bunch. Because the charge bunch is located inside a perfectly conducting cylindrical pipe, the bunch is not exactly a sphere. The spectrum in Fig. 2(a) peaks around $\omega/\omega_\perp =$ 2, 4, 6, 8, ..., which is qualitatively similar to the case of an infinitely long coasting beam [3]. This is because $\omega = \omega_\perp = \omega_z$ is the only dominant characteristic frequency in the system. Because the space-charge forces depress the betatron frequency of the charged particles, the spectra peak below, instead of exactly on, the even integers. As the

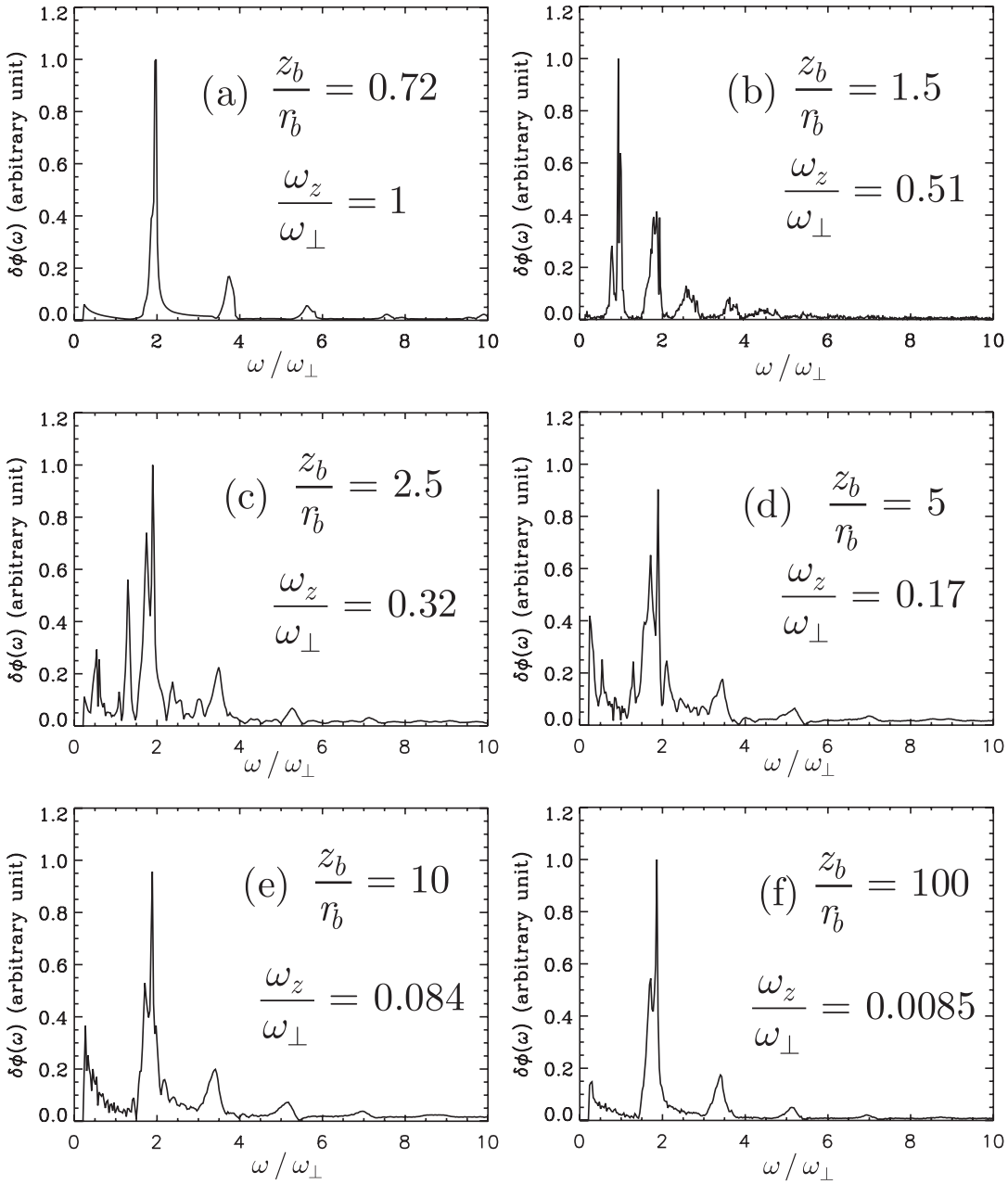

FIG. 3. Spectra of axisymmetric linear eigenmodes for bunched beams with normalized space-charge intensity $s_b = 0.5$ and different aspect ratios $z_b/r_b = 0.72$, 1.5, 2.5, 5, 10, and 100. The values of r_b/r_w are kept at $r_b/r_w = 0.26$ for all cases.

beam aspect ratio increases, additional eigenmodes emerge in between $\omega/\omega_\perp = 2, 4, 6, 8, \ldots$. For example, there is one major peak in the interval $0 < \omega/\omega_\perp < 2$ for $z_b/r_b = 1.5$ [Fig. 2(b)], and two major peaks appear in the same interval for $z_b/r_b = 2.5$ [Fig. 2(c)]. These additional modes are the result of a coupling between the transverse and longitudinal dynamics induced by the finite length of the charge bunch. As the bunch length increases, more eigenmodes appear in the intervals between even integers [Fig. 2(d)]. However, as the bunch length becomes large, these additional eigenmodes congregate towards even integers [Fig. 2(e)]. When the bunch length approaches infinity, the spectrum of an infinitely long coasting beam [3] is recovered [Fig. 2(f)]. The effects of finite bunch length are clearly evident from the fact that the spectra for an infinitely long coasting beam and a nearly spherical charge bunch are qualitatively similar, and the fact that the spectra undergo significant changes when the bunch length varies between these two limiting cases.

Similar behavior of the spectra is also found at higher space-charge intensity. Plotted in Fig. 3 are the spectra for the case where $s_b = 0.5$ for different bunch lengths. The basic features observed for the case where $s_b = 0.27$ in Fig. 2 are still evident in Fig. 3. By comparison, we observe that higher space-charge intensity produces a larger spread in the spectral peaks, and as a consequence, different eigenmodes are coupled more effectively. The width of the spectral peaks corresponds to damping in the time domain, which is likely a manifestation of the effects of space charge on collisionless damping of the mode excitations, caused by Landau damping due to wave-particle interactions and by the spatial spread in (depressed) transverse and longitudinal betatron frequencies. The larger the space-charge intensity, the stronger the damping of the collective excitations.

To further understand the interplay between space-charge effects and finite bunch-length effects, we turn to the simulation results presented in Fig. 4. Shown in Fig. 4 are the spectra for bunches with the same aspect ratio $z_b/r_b = 1.5$, but different space-charge intensities corresponding to $s_b = 0.01$, 0.27, 0.5, and 0.8. Figure 4(a) corresponds to the case where $s_b = 0.01$, in which the space-charge effects are reduced to a minimum. Because the space-charge spreading of the spectral peaks is minimized, families of eigenmodes are clearly revealed. As the space-charge intensity increases, the spread "smears out" the families of eigenmodes. For a bunched beam with high space-charge intensity at $s_b = 0.8$ [Fig. 4(d)], discrete eigenmodes can hardly be recognized, except for the first several major peaks.

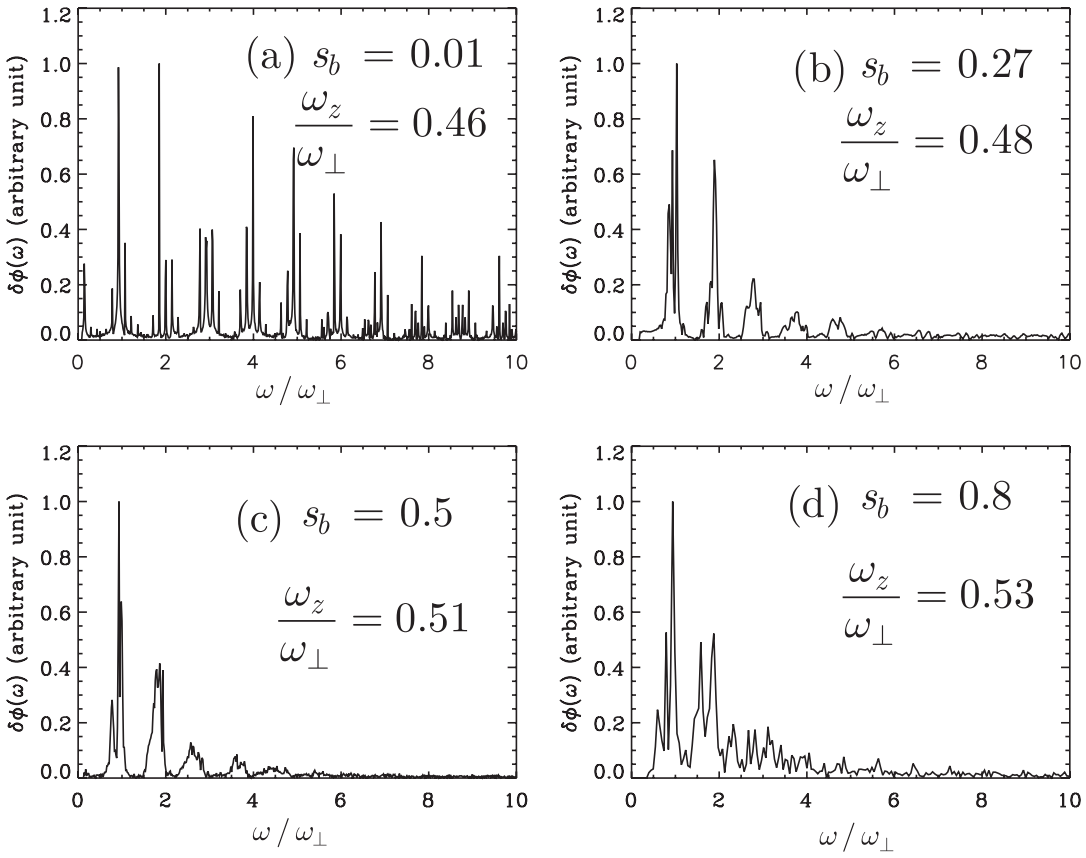

FIG. 4. Spectra for charge bunches with the same aspect ratio $z_b/r_b = 1.5$, but different normalized space-charge intensities corresponding to $s_b = 0.01$, 0.27, 0.5, and 0.8. The values of r_b/r_w are 0.33, 0.35, 0.26, 0.24, respectively.

IV. COLLECTIVE EXCITATIONS FOR BUNCHED BEAMS WITH ENERGY ANISOTROPY

Energy anisotropy develops naturally for charged particle beams due to phase space volume conservation when the beam is accelerated [2]. To model bunched beams in accelerators, it is desirable to consider equilibria with anisotropic temperature in the transverse and longitudinal directions. However, as discussed previously [36], exact kinetic equilibria do not exist for anisotropic bunched beams. Approximate kinetic equilibria with anisotropic energy can be constructed for long bunches, or other cases where the coupling induced by the nonlinear space-charge field is relatively weak. For these cases, the transverse energy $H_\perp$ and longitudinal energy H_z defined by

$$H_\perp = \frac{p_\perp^2}{2m} + \frac{m}{2}\omega_\perp^2 r^2 + e\tilde{\phi}_0(r,z), \tag{19}$$

$$H_z = \frac{p_z^2}{2m} + \frac{m}{2}\omega_z^2 z^2 + e\langle\phi_0\rangle(z), \tag{20}$$

are approximately conserved [36]. Here, $\langle\phi_0\rangle$, $\tilde{\phi}_0$, and $\overline{\phi_0}$ are defined by

$$\langle\phi_0\rangle(z) = \overline{\phi_0}(z) - \overline{\phi_0}(0), \tag{21}$$

$$\tilde{\phi}_0(r,z) = \phi_0(r,z) - \langle\phi_0\rangle(z), \tag{22}$$

$$\overline{\phi_0}(z) = \frac{\int_0^{r_w} r\phi_0(r,z)dr}{r_w^2/2}. \tag{23}$$

For present purposes, we choose the reference distribution function f_0 in the beam frame to be the anisotropic thermal equilibrium distribution

$$f_0 = \frac{\hat{n}}{(2\pi mT_\perp)(2\pi mT_z)^{1/2}} \exp\left(-\frac{H_\perp}{T_\perp} - \frac{H_z}{T_z}\right). \tag{24}$$

Here, $T_\perp$ and T_z are the constant transverse and longitudinal temperatures, respectively. The reference density profile $n_0(r,z)$ and reference potential $\phi_0(r,z)$ are determined self-consistently from Eq. (10).

There are two terms that determine the dynamics of w in Eq. (5). The $(df_0/dt)_\delta$ term is explicitly related to the perturbed fields, and the second term $(df_0/dt)_0$ is related to the fact that the reference state f_0 is not an exact equilibrium solution of the Vlasov-Maxwell equations. To carry out the δf particle simulations, we need to calculate the $(df_0/dt)_0$ term first. Some straightforward algebra gives

$$\frac{1}{f_0}\left(\frac{df_0}{dt}\right)_0 = -\frac{\dot{H}_\perp}{T_\perp} - \frac{\dot{H}_z}{T_z} = \dot{H}_z\left(\frac{1}{T_\perp} - \frac{1}{T_z}\right), \tag{25}$$

where

$$\dot{H}_z = ev_z\frac{\partial\tilde{\phi}_0(r,z)}{\partial z}, \tag{26}$$

and the superscript dot $\dot{}$ denotes $(d/dt)_0$. For a well-chosen reference state (f_0, ϕ_0), the dynamics associated with $(df_0/dt)_0$ has a longer time scale for variation than that of $(df_0/dt)_\delta$. A typical simulation result is shown in Fig. 5 for the case where $s_b = 0.27$, $z_b/r_b = 10$, and $T_z/T_\perp = 0.1$. For this choice of parameters corresponding to relatively low beam intensity, the charge bunch does not exhibit the Harris instability [30–33]. The separation of time scales is clear in Fig. 5. The fast time-scale dynamics is dominantly the $\omega \approx 2\omega_\perp$ collective excitation, and the slow time-scale dynamics is associated with $(df_0/dt)_0$ and the overall nonlinear evolution of the system. When $t \to \infty$, the perturbation relative to the reference state nonlinearly approaches a quasi-steady state. The perturbed potential $\delta\phi$ at the quasi-steady state is plotted in Fig. 6 as a function of (r,z). The perturbed potential and fields at quasi-steady state, combined with the reference state, gives a more accurate quasiequilibrium for the anisotropic charge bunch.

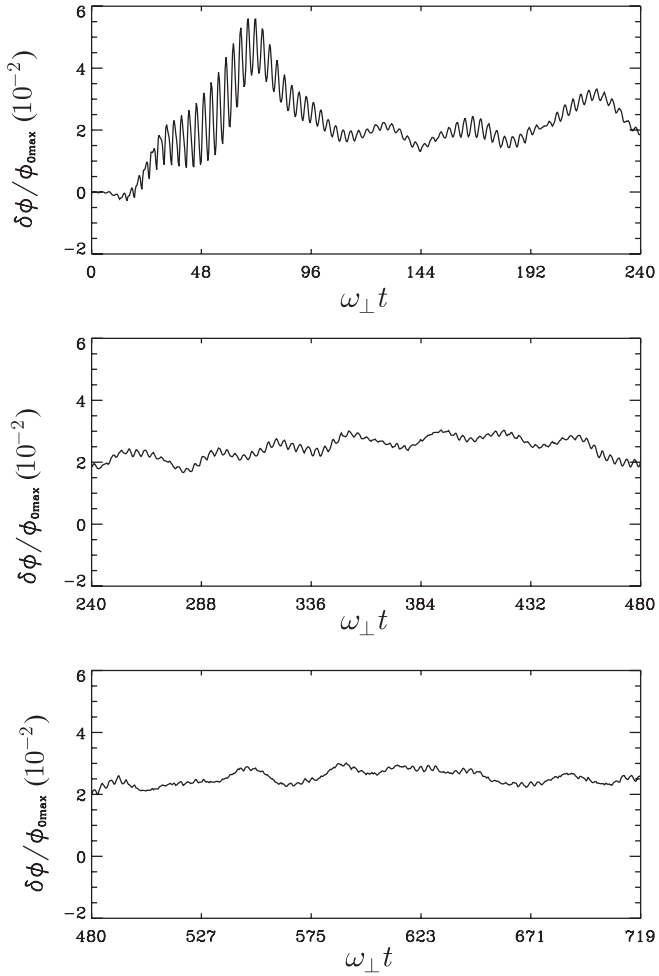

FIG. 5. Evolution of $\delta\phi$ at one spatial location $(r/r_w, z/z_{\max}) = (0.1, 0.5)$ for the case where $s_b = 0.27$, $z_b/r_b = 10$, $T_z/T_\perp = 0.1$, $r_b/r_w = 0.35$, $z_b/z_{\max} = 0.36$, and $\omega_z/\omega_\perp = 0.039$.

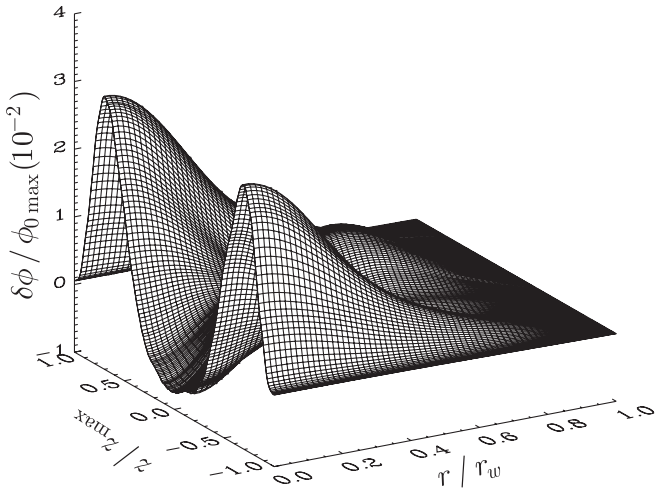

FIG. 6. Quasi-steady-state perturbed potential $\delta\phi$ as a function of (r, z).

As another application of the general δf particle simulation method for bunched beams, we present here initial simulation results for the electrostatic Harris instability driven by large temperature anisotropy in a finite-length charge bunch. The large temperature anisotropy characteristic of charged particle beams in particle accelerators has long been thought as a possible free energy source to drive collective instabilities. Recently, a systematic study has been carried out for this instability in long coasting beams [30–33], showing that both sufficiently large temperature anisotropy (small $T_z/T_\perp$) and sufficiently large beam intensity (s_b) are required for instability. The essential physics of this instability is the coupling between the transverse and longitudinal particle dynamics. For long coasting beams, the coupling is provided by the wave excitation generated by the instability. For bunched beams, the reference state for a finite-length charge bunch provides an extra channel for the coupling to take place. Indeed, we expect to see additional features of the instability due to the finite bunch length.

Shown in Fig. 7 is the time history of an unstable, azimuthally symmetric perturbation relative to the reference state (f_0, ϕ_0) at one spatial location $(r/r_w, z/z_{\max}) = (0.1, 0.5)$ for a high-intensity anisotropic charge bunch with $s_b = 0.8$, $T_z/T_\perp = 1/36$, and $z_b/r_b = 15$. The instability growth rate is measured to be $\mathrm{Im}\,\omega = \gamma = 0.25\omega_\perp$, and the real frequency is $\omega_r = \mathrm{Re}\,\omega \approx \omega_\perp$. The simulation presented here is carried out for the linear phase of the instability, using the δf method in the linearization approximation (Sec. II). Because the dynamics of the reference state associated with $(df_0/dt)_0$ is slow in comparison with the instability evolution, the $(df_0/dt)_0$ term is neglected for simplicity in the initial studies presented here. Simulations were performed for different bunch lengths corresponding to $z_b/r_b = 10$, 15, 20, 30, and 40 to investigate the effects of finite bunch length on the instability. The growth rate γ as a function of bunch aspect ratio is plotted in Fig. 8. We observe that the growth rate reaches its maximum value at $z_b/r_b = 20$ and decreases as z_b/r_b increases. The measured growth rates are somewhat larger than those in long coasting beams [30,31], which can be attributed to the stronger coupling between the longitudinal and transverse dynamics produced by the finite bunch length. The longitudinal structure of the instability shows interesting variations as well. The perturbed potential $\delta\phi$ is plotted versus the longitudinal coordinate $z/z_{\max}$ in Fig. 9 for different bunch aspect ratios. For $z_b/r_b = 10$, the unstable structure maximizes at the beam center [Fig. 9(a)]. For larger bunch aspect ratios, the unstable structure localizes symmetrically in the vicinity of

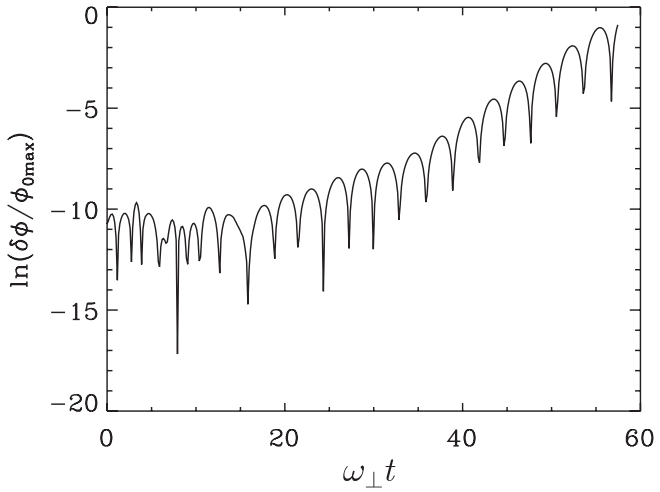

FIG. 7. Time history of an unstable perturbation at one spatial location $(r/r_w, z/z_{\max}) = (0.1, 0.5)$ for a high-intensity anisotropic charge bunch with $s_b = 0.8$, $T_z/T_\perp = 1/36$, $z_b/r_b = 15$, $r_b/r_w = 0.26$, and $z_b/z_{\max} = 0.40$.

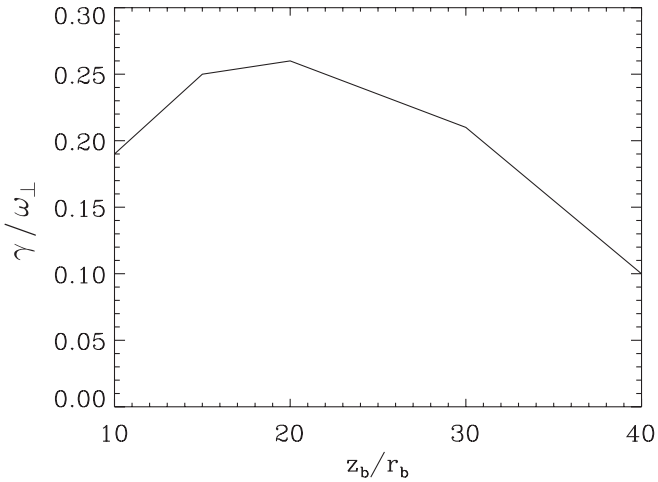

FIG. 8. Growth rate γ as a function of bunch aspect ratio z_b/r_b for a high-intensity anisotropic charge bunch with $s_b = 0.8$ and $T_z/T_\perp = 1/36$. The values of r_b/r_w and $z_b/z_{\max}$ are kept at $r_b/r_w = 0.26$ and $z_b/z_{\max} = 0.40$.

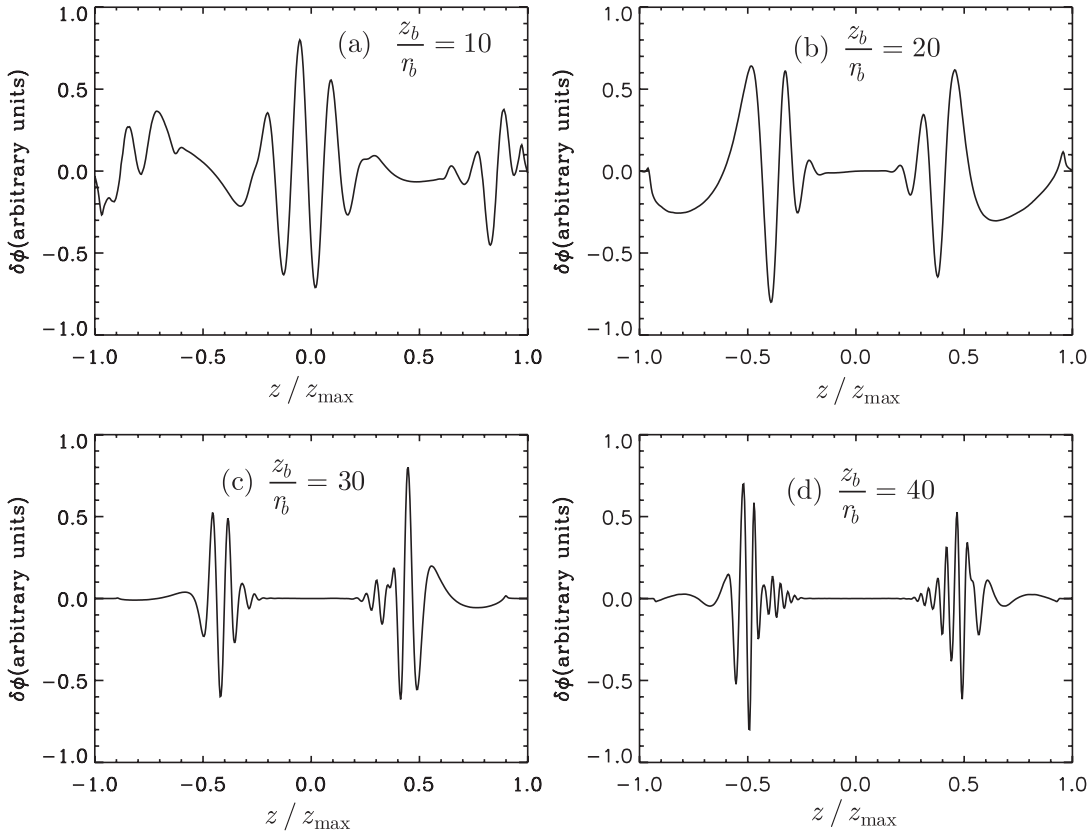

FIG. 9. Unstable perturbed potentials $\delta\phi$ (in normalized unit) as functions of z for different bunch aspect ratios with $s_b = 0.8$ and $T_z/T_\perp = 1/36$. The values of r_b/r_w and $z_b/z_{\max}$ are kept at $r_b/r_w = 0.26$ and $z_b/z_{\max} = 0.40$.

$z/z_{\max} = \pm 0.5$ [Fig. 9(d)]. The localization is more prominent for larger bunch length. As $z_b/r_b \to \infty$, the unstable structure becomes highly localized such that the beam intensity is approximately uniform across the unstable structure in the longitudinal direction, and the coupling due to the nonuniformity of the equilibrium in the longitudinal direction is significantly reduced. This explains why the growth rate decreases for increasing bunch length. In addition to the growth rate, the characteristic wave number at maximum growth in Fig. 9(d) is $k_z r_b \sim 5.2$, which agrees well with the results obtained from the study for long coasting beams [30,31].

V. CONCLUSIONS

Collective effects associated with the strong coupling between the longitudinal and transverse particle dynamics are of fundamental importance for applications of high-intensity bunched beams. In the present study, we have applied the nonlinear Vlasov-Maxwell equations to this interesting topic, and developed a generalized δf particle simulation method for high-intensity bunched beams with or without energy anisotropy. Systematic numerical studies of finite bunch-length effects on collective excitations were carried out. The finite bunch-length effect is clearly demonstrated by the fact that the spectra for an infinitely long coasting beam and a nearly spherical charge bunch are qualitatively similar, and the spectral features are distinctly different when the bunch length is varied between these two limiting cases. For bunched beams with energy anisotropy, an approximate quasiequilibrium reference state was constructed and a quasi-steady state was established in the simulations. Collective excitations relative to the reference state have also been successfully simulated using the generalized δf algorithm. In particular, the electrostatic Harris instability driven by large energy anisotropy at moderately high beam intensity was investigated in the linear regime. The observed growth rates are somewhat larger than those for infinitely long coasting beams. However, the instability growth rate decreases for increasing bunch length. For long bunches, the instability is localized symmetrically in the vicinity of $z/z_{\max} = \pm 0.5$, and the characteristic unstable wave numbers in the longitudinal direction is $k_z r_b \sim 5.2$ for the cases studied.

In future studies, we will investigate in detail the effects of spectrum spreading induced by the 3D nonlinear space-charge forces on the collective excitations. Detailed investigations of the anisotropy-driven Harris instabilities will also be carried out in the nonlinear regime, allowing for nonaxisymmetric ($\partial/\partial\theta \neq 0$) perturbations.

ACKNOWLEDGMENTS

This research was supported by the U.S. Department of Energy under Contract No. AC02-76CH03073.

[1] A. W. Chao, *Physics of Collective Beam Instabilities in High Energy Accelerators* (Wiley, New York, 1993).
[2] M. Reiser, *Theory and Design of Charged Particle Beams* (John Wiley & Sons Inc., New York, 1994).
[3] R. C. Davidson and H. Qin, *Physics of Intense Charged Particle Beams in High Energy Accelerators* (World Scientific, Singapore, 2001).
[4] I. Hofmann and J. Struckmeier, Part. Accel. **21**, 69 (1987).
[5] L. K. Spentzouris, J.-F. Ostiguy, and P. L. Colestock, Phys. Rev. Lett. **76**, 620 (1996).
[6] S. Cousineau, V. Danilov, J. Holmes, and R. Macek, Phys. Rev. ST Accel. Beams **7**, 094201 (2004).
[7] J. Struckmeier and I. Hofmann, Part. Accel. **39**, 219 (1992).
[8] V. Danilov, S. Cousineau, S. Henderson, and J. Holmes, Phys. Rev. ST Accel. Beams **6**, 094202 (2003).
[9] B. G. Logan *et al.*, Nucl. Instrum. Methods Phys. Res., Sect. A **577**, 1 (2007).
[10] R. C. Davidson and H. Qin, Phys. Rev. ST Accel. Beams **8**, 064201 (2005).
[11] H. Qin, R. C. Davidson, J. J. Barnard, and E. P. Lee, Phys. Rev. ST Accel. Beams **7**, 104201 (2004).
[12] H. Qin and R. C. Davidson, Phys. Rev. ST Accel. Beams **5**, 034401 (2002).
[13] R. Davidson *et al.*, Laser Part. Beams **20**, 377 (2002).
[14] J. J. Barnard *et al.*, Laser Part. Beams **21**, 553 (2003).
[15] R. C. Davidson, I. Kaganovich, H. Qin, E. A. Startsev, D. R. Welch, D. V. Rose, and H. S. Uhm, Phys. Rev. ST Accel. Beams **7**, 114801 (2004).
[16] R. C. Davidson, H. Qin, S. I. Tzenov, and E. A. Startsev, Phys. Rev. ST Accel. Beams **5**, 084402 (2002).
[17] H. Qin, Phys. Plasmas **10**, 2078 (2003).
[18] R. C. Davidson, Phys. Rev. Lett. **81**, 991 (1998).
[19] D. Neuffer, E. Colton, D. Fitzgerald, T. Hardek, R. Hutson, R. Macek, M. Plum, H. Thiessen, and T. S. Wang, Nucl. Instrum. Methods Phys. Res., Sect. A **321**, 1 (1992).
[20] R. J. Macek *et al.*, in Proceedings of the 2001 Particle Accelerator Conference (2001), pp. 668–672.
[21] K. Ohmi, T. Toyama, and C. Ohmori, Phys. Rev. ST Accel. Beams **5**, 114402 (2002).
[22] R. Zimmermann, Phys. Rev. ST Accel. Beams **7**, 124801 (2004).
[23] H. Qin, E. A. Startsev, and R. C. Davidson, Phys. Rev. ST Accel. Beams **6**, 014401 (2003).
[24] H. Qin, R. C. Davidson, and W. W. Lee, Phys. Rev. ST Accel. Beams **3**, 084401 (2000).
[25] R. C. Davidson, H. Qin, P. H. Stoltz, and T. S. Wang, Phys. Rev. ST Accel. Beams **2**, 054401 (1999).
[26] R. C. Davidson, H. Qin, and T. S. Wang, Phys. Lett. A **252**, 213 (1999).
[27] R. C. Davidson and H. Qin, Phys. Lett. A **270**, 177 (2000).
[28] H. Qin, R. C. Davidson, W. W. Lee, and R. Kolesnikov, Nucl. Instrum. Methods Phys. Res., Sect. A **464**, 477 (2001).
[29] H. Qin, R. C. Davidson, and W. W. Lee, Phys. Lett. A **272**, 389 (2000).
[30] E. A. Startsev, R. C. Davidson, and H. Qin, Phys. Plasmas **9**, 3138 (2002).
[31] E. A. Startsev, R. C. Davidson, and H. Qin, Phys. Rev. ST Accel. Beams **6**, 084401 (2003).
[32] E. A. Startsev, R. C. Davidson, and H. Qin, Phys. Rev. ST Accel. Beams **8**, 124201 (2005).
[33] E. A. Startsev, R. C. Davidson, and H. Qin, Phys. Plasmas **14**, 056705 (2007).
[34] C. Bohn and I. Sideris, Phys. Rev. ST Accel. Beams **6**, 034203 (2003).
[35] S. R. Hudson, H. Qin, and R. C. Davidson, Nucl. Instrum. Methods Phys. Res., Sect. A **544**, 458 (2005).
[36] H. Qin, R. C. Davidson, and E. Startsev, Nucl. Instrum. Methods Phys. Res., Sect. A **577**, 86 (2007).